Plasma-Induced, Solid-State Polymerization of *N*-Isopropylacrylamide

Alper Unver,* Guneri Akovali

Department of Chemistry, Middle East Technical University, 06531 Ankara, Turkey

Received 18 March 2008; accepted 3 September 2009
DOI 10.1002/app.31391
Published online 3 November 2009 in Wiley InterScience (www.interscience.wiley.com).

ABSTRACT: The radio-frequency plasma-initiated polymerization of *N*-isopropylacrylamide (NIPAM) in the solid state was performed. The isolated linear polymer was characterized by ^{13}C-NMR, ^{1}H-NMR, and Fourier transform infrared spectroscopy, and the effects of selected operational plasma parameters (discharge power and time) on the conversion rates were studied. Reversible transitions at the volume-phase-transition temperatures of the swelled poly(*N*-isopropylacrylamide) hydrogels were investigated by differential scanning calorimetry. The surface morphologies before and after plasma treatment were followed by scanning electron microscopy. With the obtained X-ray diffraction results, we propose a solid-state plasma polymerization mechanism for the NIPAM. © 2009 Wiley Periodicals, Inc. J Appl Polym Sci 115: 3311–3320, 2010

Key words: cold plasma; plasma polymerization; solid-state polymerization

INTRODUCTION

Polymers that respond to small changes in thermal stimulations around critical temperatures with large changes in their physical state or properties are often called *temperature-responsive polymers*.[1] In this group of polymers, poly(*N*-isopropylacrylamide) (PNIPAM) is one of the most popular because it exhibits a sharp and reversible phase transition in water at 32°C. Starting in the mid 1980s, PNIPAM has made a significant number of hits and citations in literature.[2–5] Because of its reversible thermoresponsive phase transition behavior around body temperature, PNIPAM promises big potential for a variety of novel applications, especially in biotechnology and medicine.

PNIPAM is usually used as a hydrogel and is prepared by ionizing radiation, mainly by γ radiation. On the other hand, radiation-induced, solid-state polymerization is one of the most widely studied methods in macromolecular science since the 1950s; it is based on the use of the ionizing radiation, such as X-rays and γ rays, acting as initiators or the catalyst.[6–14] Plasma is a relatively novel method used for similar purposes. Nowadays, with technologies for its applications that are becoming more practical and economical, plasma is gaining importance. With its less penetrating nature, plasma provides controllable and high quality material processing capabilities on the surface associated with low emissions of hazardous chemicals when compared with other wet-chemical methods.

One of the most widely studied monomer groups for radiation-induced, solid-state polymerization is acrylamide (AAm) and its derivatives (e.g., methacrylamide and various *N*-substituted derivatives of it). Throughout these studies, a number of different parameters affecting the polymerization kinetics have been examined, including temperature,[7,8] structure of the *N*-substituent of the monomer,[9] pressure,[10] sample preparation (e.g., crystallization rate),[11] polymerization environment (e.g., oxygen, humidity),[11] monomer orientation in the crystalline structure[12] and of the solid solution of AAm with selected monomers,[13] and nucleation and propagation of the polymerization reaction at definite imperfection sites within the crystal,[14] and all have been published and are well documented in the literature.

Although the polymerization of *N*-isopropylacrylamide (NIPAM) can be carried out with conventional polymerization methods, ionizing radiation has generally been preferred and has been distinguished as an eligible and practical tool for the synthesis of PNIPAM because of its a simplicity and because it is an additive free process where no initiator or chemical accelerators are required. Hence, use of a powerful ionizing radiation source, primarily γ, leads mainly to a residual-free crosslinked polymer with almost no linear polymer content remaining. However, the crosslinked polymer obtained also brings limited utilization with almost no processability because of its insoluble and nonfusible nature.

**Present address:* Ilko Argem A. Ş., Hacettepe Üniversitesi, Teknokent 2. Ar-Ge Binası Kat: 1 No: 15 Beytepe, Ankara, Turkey.

Correspondence to: G. Akovali (akovali@metu.edu.tr).

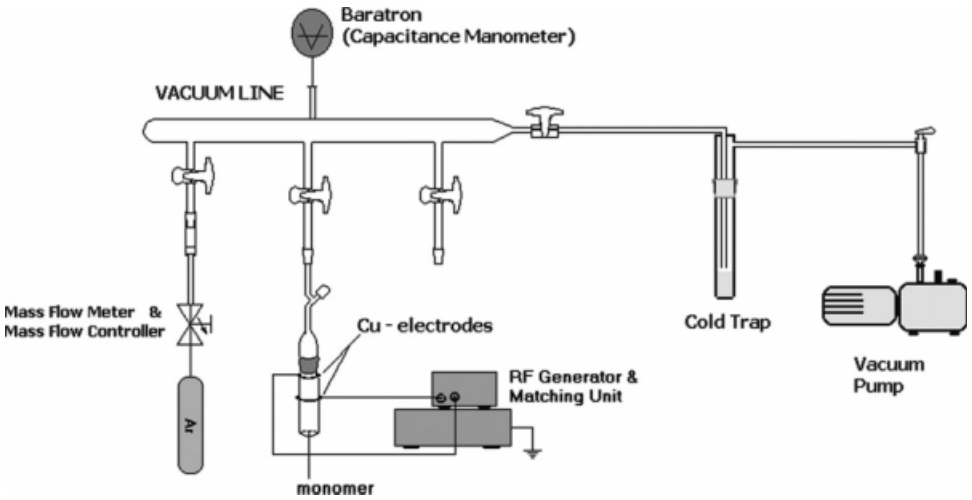

Figure 1 Low-temperature (RF) plasma-discharge system used in the monomer conversion experiments.

In this study, we used the radio-frequency (RF) plasma (glow-discharge) technique in the solid state, with the hope of producing higher proportions of linear polymer, which is more easily processable. Because the RF plasma method offers an initiator-free process under clean atmospheres (vacuumed and argon fed), a side-product-free polymer was expected as a result. In addition, the product (linear PNIPAM) and unreacted monomer residue were easily isolated by means of simple purification methods, which can be considered another advantage.

Throughout the studies, X-ray data were used to shed more light on the plasma-induced, solid-state polymerization mechanism of NIPAM, and we found that the crystalline structures of AAm and NIPAM were isomorphous.

EXPERIMENTAL

Plasma treatment of NIPAM

A schematic illustration for the setup of the low-temperature RF plasma-discharge system, with a frequency of the excitation voltage continuous at 13.56 MHz, prepared for the weight conversion experiments, is given in Figure 1. The power supply used (Tegal product, Petaluma, CA) was operated between 1 and 40 W for the proposed reactor and the ring electrodes presented. A capacitance manometer (Baratron) and its readout unit were used for vacuum-level monitoring of the plasma media. The monomer NIPAM (97%) was purchased from Aldrich (Germany), which was further recrystallized from deionized water *in vacuo* just before plasma discharge.

Argon (Ar) was used as the working gas during the plasma processes, and its glow was maintained over the surface of the pure crystalline monomer of NIPAM. By keeping several operational parameters constant, such as the reactor and electrode geometry, amount of the monomer (0.5 g for each charge), flow rate, and pressure, for all sets of the experiments, we inspected the dependence of monomer conversion on the plasma power and plasma-discharge time separately. In the light of data obtained from the diagnostic studies, two different plasma-discharge durations (1 and 5 h), and two different RF powers (20 and 40 W) were chosen.

Determination of the monomer conversions

Throughout the study, the percentage weight conversions of monomer to polymer were measured after the utilization of certain dissolution and extraction methods applied successively, as explained later: After each plasma treatment, a mixture of unreacted monomer and linear and crosslinked polymer was obtained, and these contents were further isolated by means of several physical and wet chemical techniques, such as filtration and water–ether heterogen extraction medium applied step by step, as schematized in Figure 2. In this multistep isolation method, first, the insoluble crosslinked polymer was separated by filtration from an aqueous solution of the raw product mixture. Second, the unreacted monomer was isolated from a diethyl ether–water heterogeneous system.

After isolation, evaporation, and desiccation of each component, all constituents were dried under reduced pressure to a constant weight; then, their percentage weight values were calculated gravimetrically for all of the components (monomer, linear polymer, and crosslinked polymer) separately. In addition, the unreacted monomer contents were determined quantitatively by the well-established bromide–bromate titration (volumetric) method.[15,16]

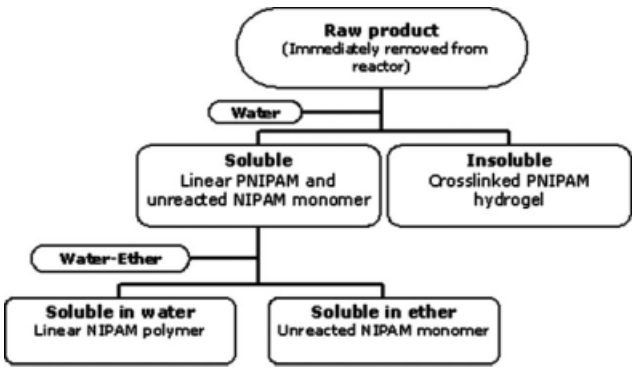

Figure 2 Block diagram of the isolation procedure for the solid-state plasma-initiated PNIPAM.

Fourier transform infrared (FTIR) measurements

FTIR analyses of components isolated from the final product mixture of the solid-state-polymerized NIPAM were performed with a Bruker Vertex 70 (Bruker Optik GmbH, Ettlingen, Germany). After plasma treatment, the samples were composed of highly crosslinked polymer at the surface, and this polymeric content was carefully isolated as a film. FTIR samples were prepared in potassium bromide (KBr) pellets by help of a KBr pellet die kit and analyzed. The spectra taken by the FTIR system were recorded in the frequency region from 4000 to 700 cm^{-1}. Each spectrum was collected at a spectral resolution of 8 cm^{-1} in transmission mode, and 20 scans were averaged per spectrum. From the spectra obtained, the plasma effect was elucidated in detail.

NMR studies

In this study, ^{13}C-NMR and ^{1}H-NMR spectra were recorded on a Bruker Spectrospin Avance DPX400 Ultrashield (^{13}C-NMR: 100 MHz and ^{1}H-NMR: 400 MHz) spectrometer. In all sample preparations for NMR study, D_2O was used as the solvent.

Differential scanning calorimetry (DSC) analysis of the PNIPAM hydrogels

Measurement of the volume-phase-transition temperature (VPTT) of the PNIPAM hydrogels and lower critical solution temperature (LCST) of linear correspondent were determined with a TA-Modulated DSC V4.1C DuPont 2000 (TA Instruments, New Castle, DE). All hydrogels were immersed in deionized water at room temperature and allowed to swell for at least 30 min to reach a certain swelling level. The thermal analyses were performed from 25 to 40°C at a heating/cooling rate of 2°C/min on the swollen hydrogels under a nitrogen atmosphere. Deionized water was used as the reference in the DSC measurements.

Scanning electron microscopy (SEM)

The visual investigation of the surface morphology of the crystalline monomer before and after plasma treatment was done with SEM micrograms, which were taken on a Stereoscan S4-10 electron microscope (Cambridge Scientific Instruments Limited, Cambridge, England). Samples were prepared in three sets, that is, recrystallized monomer with no plasma treatment, a sample after RF discharge treatment at 30 W for 1 h, and the solid-state, plasma-polymerized linear PNIPAM (preconcentrated on the holder drop by drop from its isolated aqueous solution).

X-ray diffraction (XRD) studies

XRD patterns were taken by Rigaku Miniflex (Kent, England) diffractometer with Cu Kα radiation (30 kV, 10 mA, $\lambda = 1.54051$ Å). Scanning was performed between $5° < 2\theta < 60°$ with a 1°C/min scanning rate.

RESULTS AND DISCUSSION

In-source plasma monomer conversion rates

In this part of the study, crystalline monomer samples processed in plasma at several selected different plasma durations and plasma powers (1, 3, and 5 h and 20 and 40 W, respectively) were immediately analyzed. The results obtained from the volumetric method are presented in Figure 3 as the percentage loss of C=C unsaturation versus time of plasma discharge. In this study, the conversion data obtained by the volumetric method were found more reliable than those obtained by the gravimetric one. The

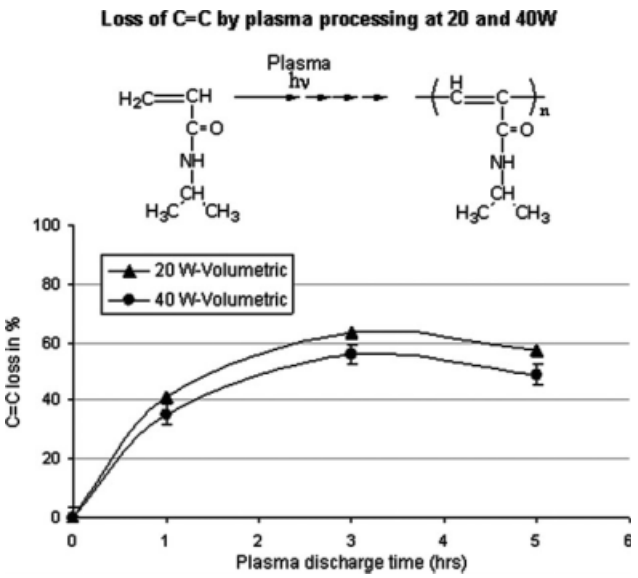

Figure 3 Volumetric (C=C) determination of monomer deprivations in percentage by plasma discharges at 20 and 40 W.

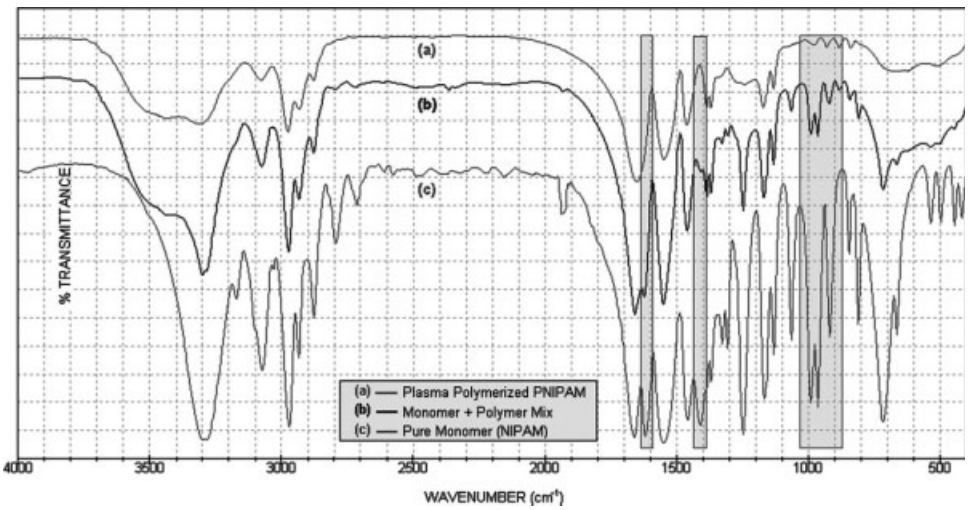

Figure 4 FTIR spectra of (a) plasma-polymerized PNIPAM polymer, (c) unreacted NIPAM monomer, and (b) a mixture of the two.

formation of very low-molecular-weight oligomeric units (dimers, trimers, tetramers, etc.) occurred in considerable amounts during plasma processing. Because the formed oligomeric molecules had very low molecular weights compared with the polymer molecules, they could not be isolated from the unreacted monomer by the applied water–ether extraction method, so this oligomeric portion was included in unreacted monomer content in the gravimetric method. On the other hand, by the bromide–bromate titration (volumetric) method, direct quantitative determination of the vinyl groups of the monomer was possible, which made this method far more trustworthy than the other.

The monomer conversions with time for both power levels applied looked similar: they increased to a certain extent and then tended to slightly decrease with increasing plasma duration. The highest conversion rates were reached within 3 h of discharge time, after which the plasma obviously caused a decrease in the conversion because of the degradative fragmentation and drop-offs in molecular weights in both cases.

At high plasma-discharge watts, that is, 40 W, an established powerful plasmon atmosphere resulted in high degradation rates that led to a large-scale decrease in the molecular weight of the polymerized portions, especially at the sample surface in direct contact with the plasma. This may have also decreased the amount of linear polymer content in regions at and nearby the surfaces in the high-watt plasma experiments.

FTIR results

Sampling was done with utmost care both from the highly polymerized and crosslinked surface and

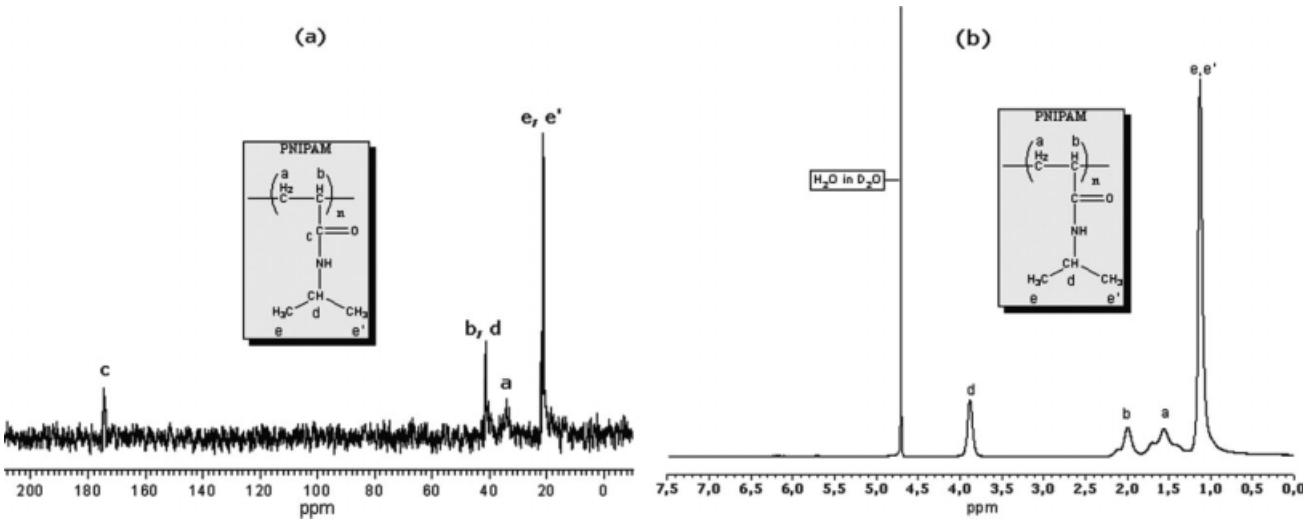

Figure 5 NMR spectra of solid-state plasma-polymerized linear PNIPAM: (a) ^{13}C-NMR and (b) ^{1}H-NMR.

TABLE I
Chemical Shifts in the ^{13}C-NMR and ^{1}H-NMR Spectra of NIPAM and PNIPAM

Sample	Spectrum	CH_3 (e or e′)	CH (b or b′)	CH (d)	CH_2 (a or a′)	CO (c)
NIPAM	^{13}C	20.92	126.37	41.31	129.87	166.81
	^{1}H	1.01	5.58	3.82	6.01	—
PNIPAM	^{13}C	21.63	41.84	41.84	34.62	175.37
	^{1}H	1.13	2.00	3.88	1.56	—

from the (partially or nonpolymerized) inner layers of the plasma-treated NIPAM. From the spectra, which is presented in Figure 4(a), common absorption bands for amide I (C═O stretching) and amide II [N—H bending (%60) and C—N stretching (%40)] bands were seen at 1651 and 1547 cm^{-1}, respectively. In addition, there were two moderately strong absorption bands at 1369 and 1389 cm^{-1}. The latter were attributed to the deformation of two methyl groups on the isopropyl [—$CH(CH_3)_2$] functionality. In light of these findings, it would not be wrong to say that the pendant group was retained apparently in the structure of plasma-induced, solid-state-polymerized PNIPAM.

As shown in the comparison of the three spectra with each other presented in Figure 4, the C═C bond absorption band observed near 1620 cm^{-1} of the pure monomer diminished over the course of monomer conversion to polymer and disappeared completely in the pure polymer spectrum. Likewise, strong bands at 1411 and at 991 cm^{-1} (with its strong overtone at 964 cm^{-1}) and another strong band at 918 cm^{-1} weakened gradually during the transition from monomer to polymer. All of these absorption bands, which are distinctive for vinyl groups, are shaded in Figure 4. These regular transformations helped somehow to strengthen the radical polymerization mechanism through the path of C═C vinyl bond cleavage.

As a result, in the course of the solid-state plasma-initiated polymerization of NIPAM, there was no appreciable loss of chemical functionality used in the final product emanating from the energetic radiation used. This may have been a result of the protection of inner layers mostly with linear PNIPAM from the destructive fragmentation under energetic plasma discharge because of the highly crosslinked layer formed on the sample surface. The low penetration nature of the plasma played another important role in the preservation of the inner layers; this led to a mostly linear polymer.

Structure elucidation by ^{13}C-NMR and ^{1}H-NMR analysis

^{13}C-NMR and ^{1}H-NMR spectra of the plasma-polymerized PNIPAM are given in Figure 5(a,b), with the peak assignments in each figure. For PNIPAM, the ^{13}C-NMR and ^{1}H-NMR spectra were obtained for the isolated polymer after plasma treatment and for the unreacted monomer, and peak assignments were done in accordance with the literature.[17–20] The observed chemical shifts are listed in Table I.

The ^{13}C-NMR spectrum of PNIPAM had the most downfield peak that could be assigned to the carbonyl carbon (C═O at δ = 175.3 ppm), followed by the main-chain methine overlapped pendant group methine (CH at δ = 41.8 ppm), the peak

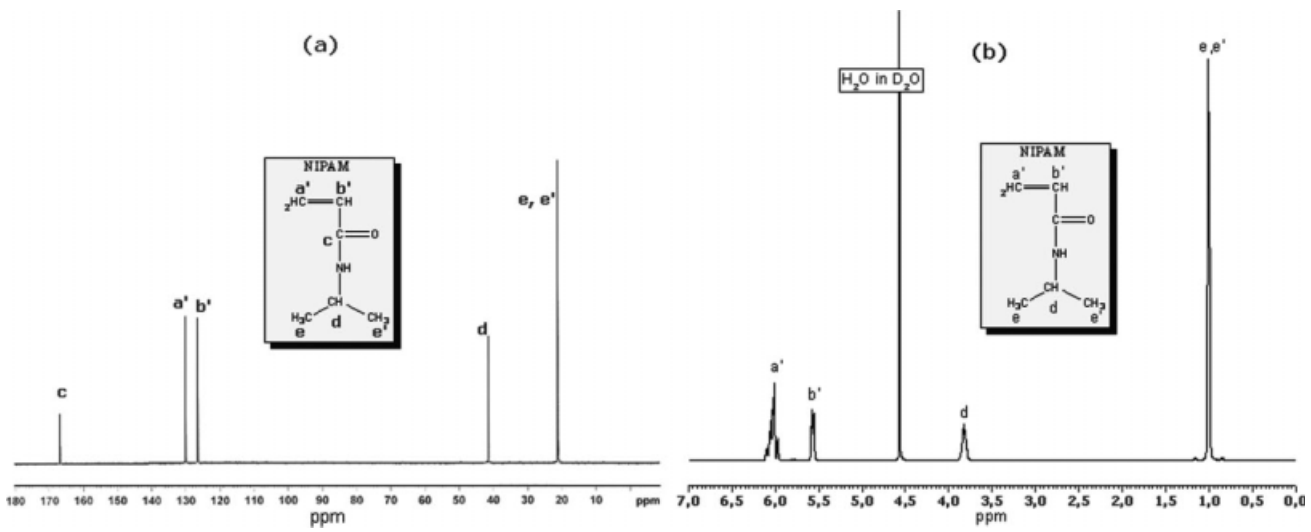

Figure 6 NMR spectra for isolated unreacted NIPAM: (a) ^{13}C-NMR and (b) ^{1}H-NMR.

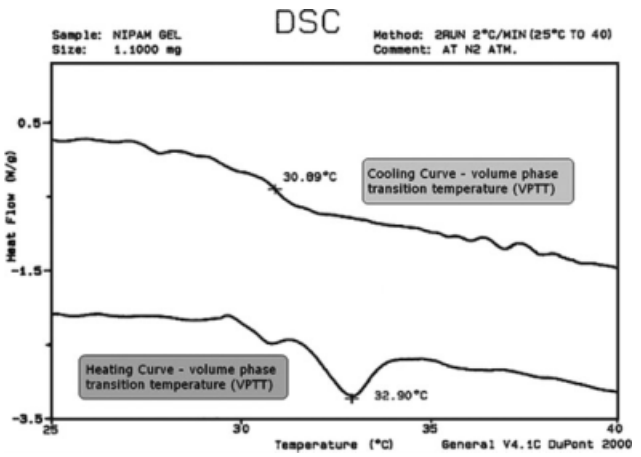

Figure 7 DSC thermogram of the solid-state PNIPAM hydrogel.

corresponding to the methylene group on the main chain (CH_2 at $\delta = 34.6$ ppm), and finally, the methyl groups of the pendant isopropyl functionality (CH_3 at $\delta = 21.6$ ppm). The structure clarified by ^{13}C-NMR was also validated further by ^{1}H-NMR [Fig. 5(b)]; there seemed to be a good correspondence between them. In the ^{1}H-NMR spectra, absorptions of unsaturated vinyl carbon protons [$\delta = 5.6$ ppm and $\delta = 6.0$ ppm in Fig. 6(b)] found in the monomer structure disappeared. Instead, proton absorptions of saturated carbons constituting the main chain were revealed with the chemical shifts of 2.0 ppm (1H) and 1.6 ppm (2H). Additionally, absorptions of 6-methyl protons (CH_3 at $\delta = 1.1$ ppm) and protons of methine (CH at $\delta = 3.9$ ppm) of isopropyl functionality were in the spectrum.

The NIPAM monomer structure was also investigated by ^{13}C-NMR and ^{1}H-NMR tests.

The ^{13}C-NMR spectrum of the NIPAM monomer is given in Figure 6(a). The methyl carbons of the isopropyl groups gave an intense signal at $\delta = 20.9$ ppm, and methine carbon absorption appeared at $\delta = 41.3$ ppm. Vinyl carbons resonated at chemical shifts of 126.4 and 129.9 ppm successively. Finally, the least shielded carbonyl carbon absorbed at $\delta = 166.8$ ppm. In the proton spectrum, the absorptions of 6-methyl protons (CH_3 at $\delta = 1.0$ ppm) and a proton of methine (CH at $\delta = 3.8$ ppm) from the isopropyl functionality were observed. Carbons of vinyl moieties of the monomer were detected as multiple peaks at $\delta = 5.6$ and 6.0 ppm.

DSC studies

The DSC thermogram, consisting of the heating and cooling curves of the PNIPAM hydrogel, is shown in Figure 7.

The temperature at the peak summits of the DSC endotherm refers to the VPTT of hydrogel. As shown by the DSC thermogram, the PNIPAM hydrogel sample exhibited a similar VPTT around 32 ± 1°C in the cooling and heating operations, and there was good agreement with the value in literature (i.e., 32°C); a variation of ±1°C was attributed to a difference in the thermal transport rates of deionized water in the reference cell and the hydrogel filled with deionized water in the sample cell. The isolated solution of the linear polymer in water, which was totally transparent at room temperature, became translucent when heated. This was an indicator of transition at LCST.

SEM studies

The SEM micrograph of the monomer samples before and after plasma treatment are presented in Figure 8(a,b). From the beginning, we saw that the crystalline structure of monomer had a

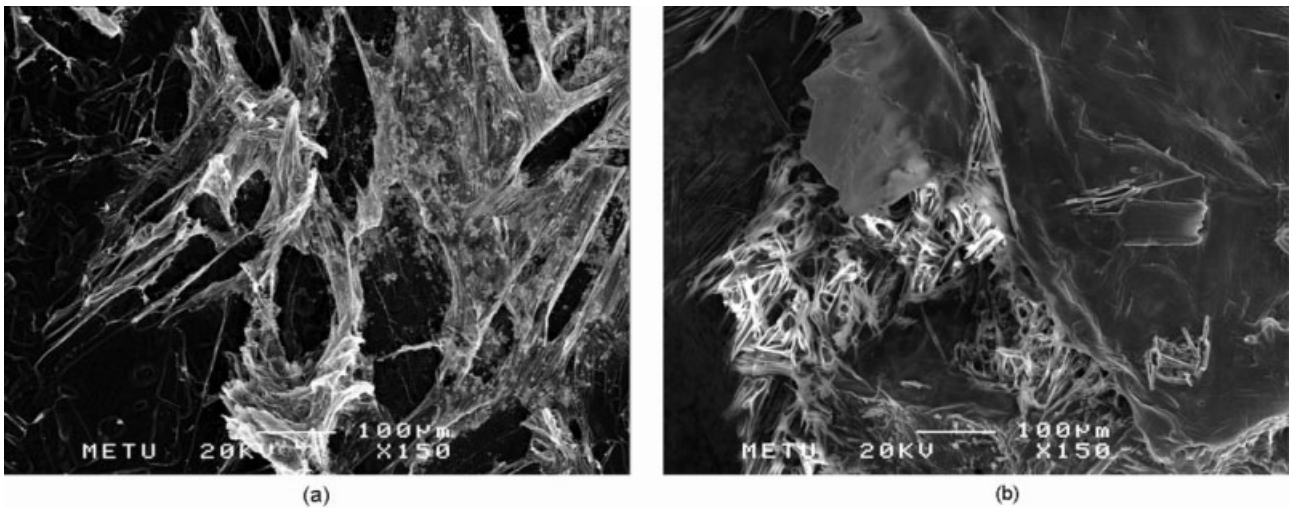

Figure 8 SEM micrographs of the crystalline monomer (a) before and (b) after plasma treatment.

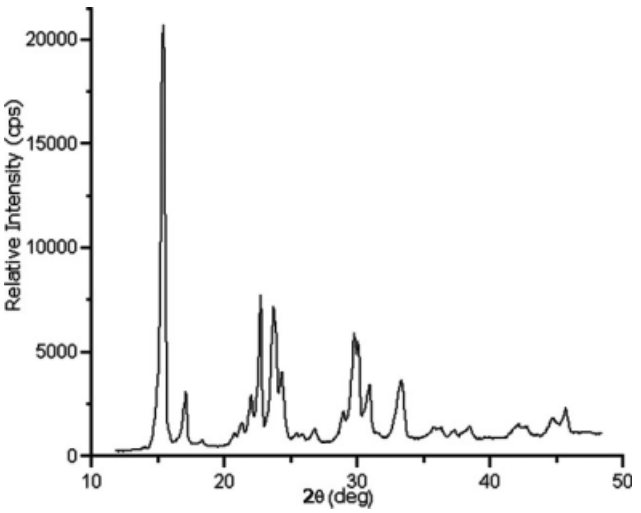

Figure 9 XRD pattern of NIPAM.

characteristic, roughly rugged (crispy) surface morphology. There were plenty of defects, ultramicrocracks due to stress-induced deformations and dislocation networks formed during crystal growth, especially located at the block boundaries in such a real crystal structure. These defects could either promote or slow down the polymerization reaction. The micrograph given in Figure 8(b) illustrates the plasma effect on the surface morphology of the sample after a discharge of 30 W for 1 h, which helped us deduce the fact that the plasma was intensively effective on the surface of the crystalline monomer flakes.

X-ray studies

The XRD patterns of the NIPAM monomer and isolated PNIPAM polymer (linear and crosslinked hydrogel forms) recorded are depicted in Figures 9 and 10, respectively.

As evidenced from the XRD patterns, the monomer NIPAM had a highly crystalline structure (with a good number of sharp peaks; Fig. 9).

However, as somewhat expected, a broad peak in the spectra of both the crosslinked and linear PNIPAMs indicated that these polymers were in the amorphous state. The samples whose XRD patterns presented in Figure 10 were extracted from the final product mixture (where the monomer was completely removed) and cast onto a glass holder before these measurements.

Although, for a polymerization proceeding in the crystalline state, it might be expected that a single crystal of polymer would be obtained from a single crystal of monomer, a number of solid vinyl monomers produced only amorphous polymers. It is generally believed that both the in-source and postirradiation results can be explained on the basis of a solid-state nucleation phenomenon, in which imperfections and defects, especially located in the borders and edges between crystal domains in the total structure, play a predominant role. There is a bit more free volume at those sites, which leads to somewhat freer thermal motion and diffusion than in the oriented lattice.[21] Because of this, the initiation (or nucleation) takes place a bit more easily at such imperfection and defect sites. In such cases, the nucleation rate is very sensitive to the concentration of such imperfections.[22]

In this study, we suggest that the plasma-induced solid-state polymerization of crystalline NIPAM was a heterogeneous reaction proceeding via a two-phase mechanism. Therefore, the amorphous polymer was obtained from the polymerization of the monomer in a crystalline state. This phenomenon is also called a *diffusion-controlled mechanism*. Once the nuclei of the reaction-product phase (a dimer) were formed, the reaction proceeded at the interface of the reagent and product phases, which were crystalline and amorphous, respectively.

It is known that AAm, which is the most extensively studied monomer in the radiation-induced, solid-state polymerization literature, follows a diffusion-controlled polymerization mechanism after its first dimerization step. Moving from the structural similarity existing between AAm and NIPAM, one can also make similar predictions about the plasma-induced, solid-state polymerization of NIPAM. However, for that; first, the *d*-spacing values of both monomers should be compared: AAm data were calculated with its unit cell parameters in the literature [the crystal lattice was monoclinic, the space group was $P2_1/c$. Other cell parameters were $a = 828.0(2)$ pm, $b = 578.0(4)$ pm, $c = 974.9(2)$ pm, $\beta = 119.62(4)^\circ$,

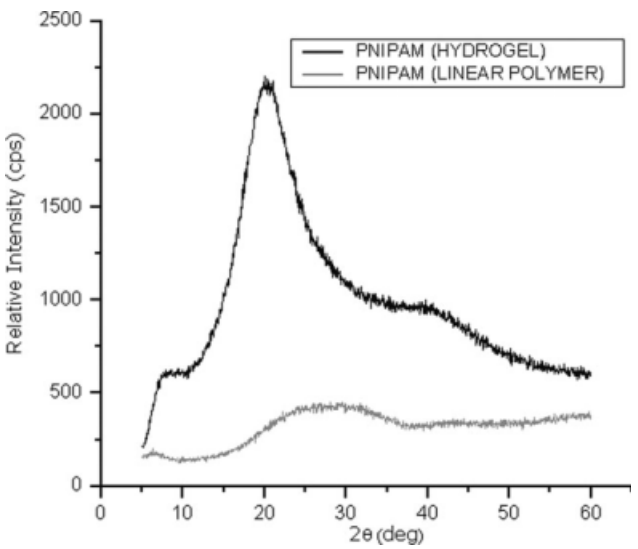

Figure 10 XRD patterns of linear and hydrogel PNIPAMs.

TABLE II
X-Ray Pattern Revealed from a Comparison of AAm and NIPAM

2θ	$1/d^2_{AAm}$	$1/d^2_{NIPAM}$	h	k	l	I/I_0
15.350	0.030	0.030	0	1	0	100
20.650	0.056	0.054	0	0	−2	2
21.300	0.059	0.058	2	0	−1	3
22.700	0.068	0.065	2	0	−2	33
23.650	0.072	0.071	1	1	−2	27
24.300	0.077	0.075	2	0	0	12
26.750	0.089	0.091	2	1	−1	3
28.900	0.105	0.105	2	0	−3	4
29.700	0.107	0.111	2	1	0	21
30.050	0.119	0.120	0	2	0	11
33.300	0.139	0.138	3	0	−1	13
33.750	0.155	0.159	0	1	−3	2
36.250	0.162	0.163	1	2	−2	2
37.250	0.170	0.172	2	0	−4	2
38.400	0.183	0.182	3	1	−3	3
42.050	0.216	0.217	1	2	−3	2
42.650	0.223	0.223	0	0	−4	2
44.650	0.245	0.243	0	2	−3	3
45.650	0.253	0.254	0	1	−4	6

h,k,l are lattice planes; d^2_{AAm} is the interplanar spacing of acrylamide d^2_{NIPAM} interplanar spacing of NIPAM; I/I_0 is the relative intensity of the reflections.

$Z = 4$ molecules/unit cell, and $d_x = 1.165$ g/cm^3 at -150°C[23], and all these d-spacing and 2θ data were compared with the values of NIPAM obtained in this study (in Table II); where ($P2_1/c$) is the monoclinic space group symbol; a,b,c is the lattice axial vectors; d is the density; β is the angle between the c and a axes; Z is the number of molecules in one unit cell; and d-spacing is the interplanar spacing. From this comparison, in fact, we saw that there was almost an entire similarity in d-spacing values at all corresponding 2θ values for both, which proved that the crystalline structures of AAm and NIPAM were isomorphous. Hence, we assumed that the plasma-induced, solid-state polymerization mechanism of NIPAM was most probably diffusion controlled, as in the radiation-induced, solid-state polymerization mechanism of AAm.

Plasma–surface interactions

It is a well-known fact that the interaction of highly energetic radiations, such as γ rays, ultraviolet (UV) rays, or X-rays, with an N-substituted AAm monomer under certain conditions (e.g., at favorable temperatures and under an inert vacuum atmosphere) gives rise to long-living excited sites with changing concentrations from the surface to the inner layers of the monomer, depending on the penetrating capacity of the irradiation. For example, highly penetrating ones (e.g., γ rays) ensure regular initiation throughout the bulk of the solid monomer, whereas in the case of UV rays (wavelength = 40–400 nm), excited site formation is concentrated mostly on the surface layers. Apart from these energetic radiations, plasma is a unique phenomenon composed from not only radiation but also highly energetic electrons at about 10^4 K and much cooler molecules and ionized species at about 300 K. Consequently, in a typical plasma-discharge medium, the excitation of monomer molecules on the surface layer is based on photons of vacuum UV (wavelength = 40–180 nm) and energetic electron bombardment emanating from the ionization of the working gas (e.g., Ar). The formation of excited sites in the solid monomer matrix surface is followed by dimerization and polymerization reactions successively. Polymerization initiated by plasma induction can be carried out by both free-radical and ionic (cationic or anionic) mechanisms. In this study, we proposed that the polymerization of vinylic NIPAM monomers in the crystalline state proceeded predominately by a free-radical mechanism because of the obtained electron paramagnetic resonance spectra of the monomer crystals exposed to RF plasma radiation, which indicated a high radical concentration. However, that will be the subject of another publication from this study.

By choosing suitable plasma process conditions, one can make optimizations to suggest a picture of glow-discharge polymerization. As shown in Figure 11, glow-discharge polymerization branched into two major types of polymerization mechanisms in this study.

One of them was plasma-induced polymerization (P-iP), and the other was plasma polymerization

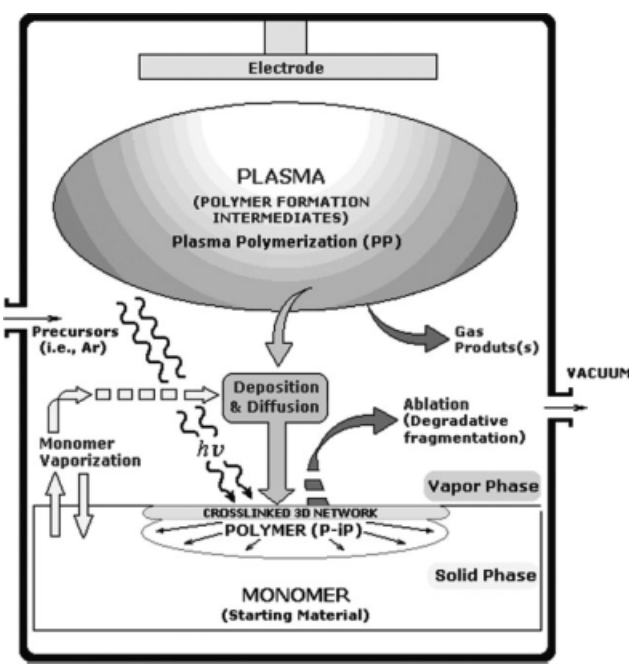

Figure 11 Overall possible interactions in the glow-discharge plasma medium.

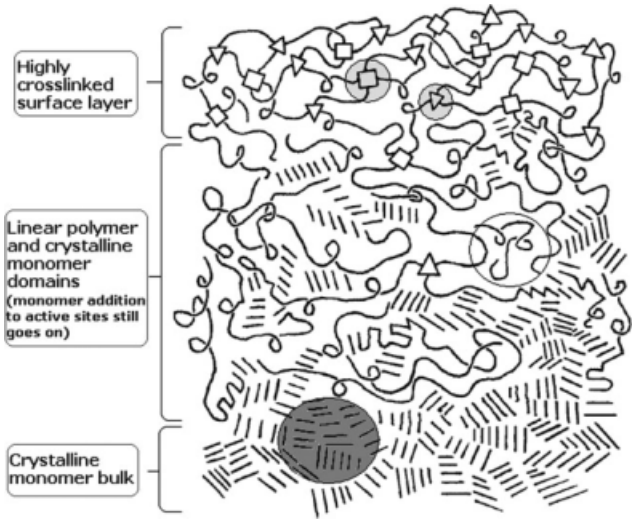

Figure 12 Proposed schematic diagram of the surface and underneath layers, including the linear polymer and crystalline monomer bulk after plasma processing.

(PP). Because of the low rate of monomer evaporation during the processing of solid NIPAM with plasma, we were not interested in the latter PP mechanism, which took place in the plasma phase. Additionally, in a plasma media, the individual steps of the reactions involved in the process of polymer formation are extremely complex. In this study, we determined that P-iP was the main mechanism, which resulted in almost all of the polymerized (linear and crosslinked) products. Therefore, our studies mainly focused on this mechanism.

In the P-iP mechanism, polymerization triggered by reactive species that were created in plasma-discharge medium resembled the conventional (molecular) polymerization reactions, where the molecular structure of the monomer was retained in the polymer formed. In this mechanism, polymerization mostly occurred on the surface of the solid monomer phase. To produce polymers by the P-iP method, the starting material must contain polymerizable structures, such as conventional olefinic double bonds, triple bonds, or cyclic structures. A representative chain propagation mechanism for P-iP in the solid state can be given as follows:[24]

$$\text{Initiation:}\quad \mathrm{M} \xrightarrow{h\nu} \mathrm{M}^* \tag{1}$$

$$\text{Propagation:}\quad \mathrm{M}^* + \mathrm{M} \rightarrow \mathrm{MM}^* \rightarrow\rightarrow \mathrm{M}_a^* \quad \text{and} \quad \mathrm{M}^* + \mathrm{M} \rightarrow \mathrm{MM}^* \rightarrow\rightarrow \mathrm{M}_b^* \tag{2}$$

$$\text{Termination:}\quad \mathrm{M}_a^* + \mathrm{M}_b^* \rightarrow \mathrm{M}_a - \mathrm{M}_b \tag{3}$$

where M is the monomer; $h\nu$ is the energetic radiation; a and b are the numbers of repeating units (i.e., $a = b = 1$ for the starting material) and M* represents reactive species, which can be an ion or either charge, an excited molecule, or a free radical produced from M. Figure 11 schematically shows the formation of a crosslinked layer on the surface by the plasma effect. The thickness of this layer depends on the rate of plasma penetration, which is approximately 100 Å. During plasma treatment, activated sites are possibly formed in this layer, and they may cause further polymerization in the solid state. This was exactly what happened in our case as well. The breaking of carbon-to-carbon bonds in the main polymer chain on the surface led to the formation of two free radicals. These free radicals could recombine, unless they were able to diffuse away from each other. If they did diffuse away, which was more probable in the surface layer than in the bulk, the molecule remained permanently broken. On the other hand, for crosslink formation, an active radical on each of two molecules had to approach to each other and react. The difficulty was that the free radicals may have been attached to large molecule fragments embedded in an entangled medium. For that reason, the crosslinking procedure predominantly occurred in the surface layer.

Below the surface layer, radicals and excited sites were protected from the outer atmosphere, and depending on the orientation of the monomer molecules, polymerization may have continued to the extent of residual linear polymer chains. In the light of the data obtained, changes in the surface regime and in the layers underneath during plasma discharge was proposed, as shown in Figure 12.

Especially in the network structure of the surface layer, there were chemical crosslinks with trifunctional and tetrafunctional network junctions (darker circles). In deeper layers, oligomers and linear polymer chains were frequently found between the monomer crystal domains (lighter circles). Some entanglements can act as physical crosslinks in these amorphous polymer domains. The possible post PP reactions in solid state can take place between the interface of the amorphous polymer and the crystalline monomer phases. The monomer domains were still available in the deeper layers. In the deeper layers, the nonpolymerized monomer amount became larger (darkest circle).

CONCLUSIONS

According to the spectroscopic characterization results, we propose the RF plasma technique as a novel and clean radiation-induced, solid-state polymerization method for NIPAM that leads to its crosslinked (gel) and linear polymers, both with similar thermal transition response characteristics. This method also leads to higher proportions of linear polymer, which are easily processable compared to the γ-radiation technique, which gives crosslinked polymer as a product with no processability.

As shown by the DSC studies, the PNIPAM hydrogel exhibited a similar transition, which was called a *volume-phase transition*, around 32 ± 1°C during the cooling and heating operations, and from this outcome, we can say that the crosslinked PNIPAM hydrogel showed similar thermoresponsive behavior with a linear polymer in water at LCST.

From the SEM micrographs of the samples taken before and after plasma treatment, the plasma was intensely effective on the surface of the crystalline monomer flakes. After the formation of excited sites in the solid monomer matrix surface, dimerization (nucleation) and polymerization reactions came successively. Polymerization initiated by plasma induction most probably proceeded by a free-radical mechanism.

According to the X-ray data, NIPAM and AAm were isomorphous so that the polymerization mechanisms of both monomers in the solid state were most probably alike, with solid-state polymerization mechanisms being mostly diffusion controlled.

The authors thank Nesrin Hasirci and Ali Usanmaz of Middle East Technical University, Department of Chemistry, for their help throughout the course of this study.

References

1. Hoffman, A. S. Clin Chem 2000, 46, 1478.
2. Gil, E. S.; Hudson, S. M. Prog Polym Sci 2004, 29, 1173.
3. Schild, H. G. Prog Polym Sci 1992, 17, 163.
4. Kikuchi, A.; Okano, T. Prog Polym Sci 2002, 27, 1165.
5. Galaev, I. Y.; Mattiasson, B. TIBTECH 1999, 17, H-335.
6. Adler, G.; Reams, W. J Chem Phys 1960, 32, H-1698.
7. Żurakovska-Országh J.; Gumułka A. In Proceedings of the Fourth Tihany Symposium on Radiation Chemistry; B/34. Proc 4th Tihany Symp Radt Chem Akad Kiado; Publishing House of the Hungarian Academy of Sciences: Budapest, 1976; p 401.
8. Żurakovska-Országh, J.; Gumułka, A. Radiat Phys Chem 1980, 15, 571.
9. Żurakovska-Országh, J.; Gumułka, A.; Bartnik, J. Radiat Phys Chem 1984, 23, 385.
10. Worrall, R.; Pinner, S. H. J Polym Sci 1959, 34, 229.
11. Fadner, T. H.; Morawetz, H. J Polym Sci 1960, 45, 475.
12. Restaino, A. J.; Mesrobian, R. B.; Morawetz, H.; Ballantine, D. S.; Dienes, G. J.; Metz, D. J. J Am Chem Soc 1956, 78, 2939.
13. Adler, G. J Chem Phys 1959, 31, 848.
14. Baysal, B.; Adler, G.; Ballantine, D.; Colombo, P. J Polym Sci 1960, 44, 117.
15. Siggia, S. Quantitative Organic Analysis via Functional Groups, 3rd ed.; Wiley: New York, 1966.
16. Lucas, H. J.; Pressman, D. Ind Eng Chem Anal Ed 1938, 10, 140.
17. Mattiasson, B.; Kumar, A.; Galaev, I. Y. J Mol Recognit 1998, 11, 211.
18. Han, S. J.; Yoo, M. K.; Sung, Y. K.; Lee, Y. M.; Cho, C. S. Macromol Rapid Commun 1998, 19, 403.
19. Díez-Peña, E.; Quijada-Garrido, I.; Barrales-Rienda, J. M.; Wilhelm, M.; Spiess, H. W. Macromol Chem Phys 2002, 203, 491.
20. Zeng, F.; Tong, Z.; Feng, H. Polymer 1997, 38, 5539.
21. Morawetz, H. Science 1966, 152, 705.
22. Adler, G.; Reams, W. J Chem Phys 1960, 32, 1698.
23. Usanmaz, A. Turkish J Chem 1997, 21, 304.
24. Yasuda, H. In Thin Film Processes; Vossen, J. L.; Kern, W., Eds.; New York: Academic, 1978; p 361.